Express Polymer Letters Vol.17, No.3 (2023) 268–289
Available online at www.expresspolymlett.com
https://doi.org/10.3144/expresspolymlett.2023.20

Research article

The effect of functionalized hydroxyapatite on the crystallization process, morphology and thermomechanical properties of polyoxymethylene composites

Klaudia Król-Morkisz[1], *Monika Kuźnia*[2], *Zbigniew Olejniczak*[3], *Małgorzata Lekka*[4], *Kinga Pielichowska*[1*]

[1]AGH University of Science and Technology, Faculty of Materials Science and Ceramics, Department of Biomaterials and Composites, al. Mickiewicza 30, 30-059 Kraków, Poland
[2]AGH University of Science and Technology, Faculty of Metals Engineering and Industrial Computer Science, Department of Heat Engineering and Environment Protection, Al. Mickiewicza 30, 30-059 Krakow, Poland
[3]Institute of Nuclear Physics Polish Academy of Sciences, ul. Radzikowskiego, 152, 31-342, Kraków, Poland
[4]Department of Biophysical Microstructures, Institute of Nuclear Physics, Polish Academy of Sciences, PL-31342 Krakow, Poland

Received 7 April 2022; accepted in revised form 28 September 2022

Abstract. In this work, hydroxyapatite (HAp) was functionalized by using poly(ethylene glycol) (PEG) with different average molar mass and diisocyanates as linkers and then incorporated into the polyoxymethylene (POM) matrix by means of melt processing methods. The effectiveness of the functionalization process and the chemical structure of the obtained hybrid systems were analyzed using thermogravimetric analysis (TG), elemental analysis, and nuclear magnetic resonance (NMR) methods. In the next stage of research, the calculation of the POM crystallization kinetic parameters in the presence of the hybrid filler were calculated. Microscopic and dynamic mechanical analysis (DMA) tests, as well as ^{13}C and ^{31}P and nuclear magnetic resonance (NMR) analyses were done to show the effect of the HAp-*g*-PEG hybrid filler on the crystallization kinetics and crystallinity of the POM composites. Transmission electron microscopy (TEM) confirmed the uniform distribution of the HAp-*g*-PEG hybrid additives. Differential scanning calorimetry (DSC) tests did not show any significant effect on the key processing parameters, *i.e.* melting point and supercooling, which allowed the processing parameters to be maintained for all samples. The study of crystallization kinetics showed a three-dimensional process of POM crystals' growth in the form of spherulites. The addition of HAp-*g*-PEG to POM significantly accelerated the crystallization process.

Keywords: *polyoxymethylene, functionalization, poly(ethylene glycol), hydroxyapatite, crystallization kinetics*

1. Introduction

Polyacetals are the group of plastics obtained by the polymerization of aldehydes. The most popular polyacetal is polyoxymethylene (POM), which is obtained from formaldehyde (homopolymer) or trioxane (copolymer) [1, 2]. POM is also called polyacetal or acetal resin and is a semicrystalline thermoplastic polymer. POM may be in the form of a homopolymer having the general formula $–(CH_2–O)_n–$ or a copolymer of the formula $–(CH_2–O)_n–(CH_2–CH_2–O)_m–$. In practice, a copolymer is used much more frequently. Among other polymeric materials, these materials are distinguished by better performance properties, including high mechanical strength, stiffness, hardness, resistance to abrasive wear, low water absorption, good chemical resistance, and ease of processing [3]. Polyoxymethylene owes these features to the high degree of ordering of the polymer chains, which

*Corresponding author, e-mail: kingapie@agh.edu.pl

is possible because of their simple, regular, and linear structure. POM is a linear semicrystalline polymer with a high degree of crystallinity ranging from 50 to 80% for polymers prepared and used on an industrial scale. The conditions that prevail during POM crystallization strongly affect the amount and morphology of the crystalline phase formed. POM chains crystallize in the hexagonal (9/5) system, creating a stable α phase, and in the orthorhombic (2/1) system leading to a metastable β phase. A POM elementary cell crystallizing in a hexagonal system has dimensions $a = b = 4.45$ Å, $c = 17.3$ Å, and contains nine monomer units derived from one polymer chain. POM crystallizes in hexagonal form from the melt or from dilute solutions. The orthorhombic form of POM is characterized by the structure of an elementary cell consisting of two polymer chains, with two mers from each chain in the elementary cell with dimensions $a = 4.77$ Å, $b = 7.65$ Å, $c = 17.80$ Å. Orthorhombic POM can be obtained by polymerization from a liquid basic solution of formaldehyde. However, the orthorhombic form of POM is metastable and transforms into a stable hexagonal form at 69 °C [4]. In POM, the orthorhombic phase is the high-density crystalline with the high compactness of 2/1 helices along the c axis, while the less dense hexagonal phase which is less stable at a lower temperature (below ca. 70 °C) and which is the most stable phase at higher temperatures. In some cases, due to kinetic reasons, thermodynamically permitted processes may be hindered, and it can lead to the formation of less thermodynamically stable products. For instance, orthorhombic POM formation was found during polymerization at a temperature below 70 °C. Below 70 °C orthogonal form is the most stable and formed faster than the less stable hexagonal form. On the other hand, during POM crystallization from the melt, mainly the formation of the hexagonal phase was found since crystallites are formed rapidly during cooling at temperature higher than 70 °C. For the transition of orthorhombic to hexagonal form, a slight expansion along the *b* axis and *a* contraction along the a axis of the orthorhombic phase is necessary.

According to these changes and distortion, the inverse hexagonal to orthorhombic forms transformation is theoretically possible by cooling the POM to a temperature below 70 °C; however, it has not been observed in practice. This effect was attributed to the hindering of necessary structural changes or extremely slow transformation at low temperatures and pressure [5]. Therefore, each thermal treatment, including processing, causes the POM used to be only in the hexagonal form [6].

POM chains form crystals with two morphological forms during crystallization. The first is extended chain crystal (ECC), the second is folded chain crystal (FCC). POM chains, under appropriate conditions, can also form shish-kebab structures, where FCC crystallize around a core made of a single ECC. ECCs are less stable, formed and melt at around 140 °C, unlike FCCs that melt at around 156 °C [7, 8]. The cationic polymerization of 1,3,5-trioxane promotes the formation of crystallites in the form of whiskers. ECC POM crystallites can also be obtained by the electrospinning method. In the case of POM crystallization from solution and melt, the folded POM chains form lamellar structures composed of a single layer with a thickness of approximately 100 Å [9].

The crystallization behaviour of POM in the presence of different nanoparticles has recently been investigated [10]. Hence, Zeng *et al*. [11] investigated the effect of silver nanoparticles on non-isothermal crystallization behavior of POM using Jeziorny, Jeziorny-modified Avrami, Ozawa, Liu, and Mo, Ziabicki, and Kissinger models. They revealed that small amounts of Ag nanoparticles incorporated into the POM matrix act as nucleating agents and could enhance the crystallization rate of POM and increase the number of growing POM spherulites with simultaneous reduction of POM spherulites size. The incorporation of higher content of Ag nanoparticles leads to their aggregation and hindrance of POM crystallization. Slouf *et al*. [12] studied POM composites with talc micropowder (POM/mTalc), chalk nanopowder (POM/nChalk), and titanate nanotubes (POM/TiNT). They revealed that the crystallization half-times change in the following order: POM/nChalk < POM/mTalc < POM/TiNT ~ POM and mTalc and nChalk are strong nucleating agents. POM with graphene nanoplatelets (GNP) was investigated by de Souza Santos *et al*. [13]. It has been found that incorporating GNP hinders the polymer crystallization process, changes the degree of crystallinity, and increases the crystallization temperature. The authors suggested that GNP acts as a nucleating agent for POM. Another approach was presented by Jiao *et al*. [14] investigated the crystallization behavior of POM in the presence of a small amount of ionic liquid – tributyl(octyl)phosphonium bis(trifloromethanesulfonyl)imide (TBOP-TFSI) – as a

nucleating agent. The differential scanning calorimetry (DSC) results and microscopic observations in polarized light showed that the incorporation of TBOP-TFSI induces crystal nucleation and formation of fine crystal grains of POM, which leads to significant improvement in the impact strength of POM blends.

In this work, hydroxyapatite (HAp) was functionalized with poly(ethylene glycol) (PEG) using diisocyanates as linkers. For this purpose, several different diisocyanates were used, including those for medical use, as well as PEGs with selected different average molar masses. From the obtained systems, those with the highest content of incorporated organic phase were selected based on thermogravimetric analysis (TG). The next stage of the research included analysis of POM crystallization kinetics in the presence of the hybrid filler, microscopic and dynamic mechanical analysis (DMA) tests, as well as ^{13}C NMR and ^{35}P NMR investigations to show the effect of the HAp-*g*-PEG hybrid filler on the crystallization kinetics and crystallinity of POM composites.

2. Experimental part

2.1. Materials

A commercially available polyoxymethylene copolymer (POM_C, Ultraform®, BASF) with a melt flow index (MFI) of 2,6 g/10 min was used as the matrix of polyacetal composites. Stoichiometric HAp ($Ca_{10}(PO_4)_6OH_2$) in the form of a nanopowder with a spherical nanoparticle shape and size 99% <100 nm, was the product of nGimat Co. (USA).

1,6-hexamethylene diisocyanate (HDI), 4,4′-diphenylmethylene diisocyanate (MDI), methylene bis-(4-cyclohecasamethylene diisocyanate) (HMDI) and 3-isocyanatomethyl-3,5 isocyanate, and 5-trimethylcyclohexyl (isophorone diisocyanate (iPDI)) were Sigma Aldrich products. PEG (Sigma Aldrich) with selected three different mass average molar masses – 600, 2000, and 6000 g/mol, was used to modify HAp. The catalyst, dibutyltin dilaurate (DBTL), was also manufactured by Sigma Aldrich. Dehydrated *N*,*N*-dimethylformamide (DMF), and ethyl alcohol were products of Avantor. Before the grafting process, HAp was dried at 110 °C for 2 h, and PEG was dried at 90 °C under a vacuum also for 2 h. PEG with the selected molar mass was grafted onto the HAp surface using one of the selected diisocyanates as a linker.

2.2. HAp functionalization and POM composites preparation

The process of grafting PEG chains on the HAp surface was carried out in two stages. Table 1 shows the amounts of reagents used in the grafting process. The molar ratio of HAp:diisocyanate:PEG reagents was 1:2:1.

In the first step, 9 g of HAp was gradually dispersed by sonication in a three-necked flask under a nitrogen atmosphere in 90 ml of DMF over a period of 1 h, without exceeding the suspension temperature of 30 °C. 9 µl of catalyst was then added to the obtained HAp suspension in DMF. Simultaneously, a 1:2 weight ratio of the diisocyanate in a DMF solution was prepared, which was then added dropwise to the HAp slurry. After the dropwise addition of the diisocyanate solution, over a period of about 30 minutes, the system was heated with a heating mantle and stirred with a magnetic stirrer under a nitrogen atmosphere to a temperature of 80 °C where the diisocyanate-HAp coupling reaction was carried out for 2 hours. After this time, the system was cooled to room temperature, and then the solution of PEG in DMF was added dropwise in a mass ratio of 1:1. After the PEG solution was dosed, the system was reheated to 60 °C, whereby PEG grafting reaction to isocyanate groups was performed for another 1.5 hours, and then the reaction mixture was cooled down to the room temperature. After completion of the reaction, the mixture was centrifuged using a laboratory centrifuge for 20 minutes at a speed of 4000 rpm. After centrifugation, the precipitate was washed three more times with dry ethanol. After washing and centrifuging, the material obtained was transferred to a Petri dish and dried, first for 24 h at room temperature and then for 24 h at 40 °C. After this time, the dried material was ground in a mortar and then stored in a desiccator.

Table 1. Amounts of reagents used in the PEG grafting on the HAp surface.

Nr.	HAp	Mass [g]	Diisocyanate	Mass [g]	PEG	Mass [g]
1	HAp	9.00	HDI	6.00	600	10.75
2					2000	35.83
3					6000	107.50
4			MDI	8.93	600	10.75
5			HMDI	9.36		10.75
6			iPDI	7.93		10.75

Polyacetal composites (POM/HAp-*g*-PEG) were obtained by means of two-stage melt processing – extrusion and injection moulding. After TG analysis of the obtained HAp-*g*-PEG powders, the percentage content of the inorganic phase was determined as a solid residue at a temperature of 600 °C. On this basis, the concentration of HAp was calculated in each of the HAp-*g*-PEG systems. In the next step, the blends obtained were subjected to an extrusion process to disperse HAp-*g*-PEG in the polymer – composites with HAp-*g*-PEG content 0.5; 1.0; 2.5; 5.0, and 10.0% were obtained. The extrusion process was carried out with a laboratory twin-screw co-rotating extruder (HAAKE™ MiniLab Micro Compounder) at a temperature of 210 °C, with the rotation speed of the screws 50 rpm. The injection process was carried out using a Zamak WT12 injection moulding machine. The injection process parameters were as follows: mould temperature – 90 °C, plasticization temperature – 210 °C, plasticization time – 3 minutes, injection pressure – 10 bar.

2.3. Testing methods

Thermogravimetric analysis (TGA) was performed using a Netzsch STA 449 Jupiter® thermal analyzer. Samples of ca. 10 mg were placed in open alumina crucibles. Measurements were carried out at a heating rate of 10 K/min, from 40 to 600 °C, under a nitrogen atmosphere (flow 30 ml/min). Elemental analysis of elements: carbon, oxygen, and hydrogen in HAp-*g*-PEG samples was performed with the LECO CHN628 elemental analyzer according to ASTM D 5373 standard. The test samples were burned in pure oxygen at a temperature of 950 °C to completely burn the organic part. The content of C and H in the flue gas was determined successively – based on the analysis of the infrared absorption spectra, while N – based on the measurement of thermoconductivity. NMR measurements (^{1}H MAS-NMR, ^{31}P MAS-NMR, and ^{13}C MAS-NMR) were carried out in the solid-state for HAp-*g*-PEG powders and POM_C/HAp-*g*-PEG composites. High-resolution Magic Angle Spinning (MAS-NMR) spectra in the solid state were measured on a Tecmag APOLLO spectrometer, working with a Magnex superconducting magnet with a field of 7.05 T and a diameter of 89 mm. A Bruker HP-WB MAS probe was used to spin the sample. The sample was placed in a zirconium rotor with a diameter of 4 mm, equipped with a KEL-F turbine. The free precession signal was recorded after a single excitation pulse with a length of 3 μs, corresponding to the magnetization rotation by 90°. ^{31}P MAS-NMR spectra were measured at a resonance frequency of 121.26 MHz, spinning the sample at 4 kHz. The spectrum resulted from averaging 128 measurements made with a repetition time of 10 s. The ppm scale was determined using a liquid sample of 85% H_3PO_4 solution. ^{13}C MAS-NMR spectra were measured at a resonance frequency of 75.33 MHz, while the sample was spinning at 8 kHz. The spectrum resulted from averaging 400 measurements made with a repetition time of 20 s. The ppm scale was determined using a liquid TMS (tetramethyl-silane) sample ($Si(CH_3)_4$). ^{1}H MAS-NMR spectra were measured at a resonance frequency of 299.56 MHz by spinning the sample at 8 kHz. The spectrum resulted from averaging 1000 measurements made with a repetition time of 1 s. The ppm scale was determined using a liquid TMS (tetramethyl-silane) sample ($Si(CH_3)_4$). FTIR spectra were recorded with the Vertex 70v spectrometer (Bruker) at room temperature, in the air atmosphere, with a resolution of 2 cm^{-1}, in the range of 4000–500 cm^{-1}. For HAp-*g*-PEG samples, measurement was performed using potassium bromide (KBr) pellets. For POM/HAp-*g*-PEG composites, measurements were carried out using the attenuated total reflectance (ATR) technique with the HATR PIKE attachment on a diamond crystal. The surface morphology of POM composites was investigated using a scanning electron microscope (SEM) (Nova NanoSEM 200, FEI) at an accelerating voltage of 1 kV, after previously sputtering the samples with carbon. A microscope equipped with an EDAX X-ray spectrometer (EDX) was used to analyse chemical elements on the surface of the tested samples. A TEM microscope (LEO 912AB, Carl Zeiss, Germany) was used to assess the degree of dispersion of HAp-*g*-PEG in the polymer matrix. Prior to observation, the samples were cut with an MTX ultramicrotome (RMC Products, Tucson, USA).

The DSC 1 differential scanning calorimeter (Mettler Toledo) was used for the DSC measurements. Measurements were made at a heating and cooling rate of 10 K/min in a nitrogen atmosphere (flow 30 ml/min). The samples weighing ca. 5 mg were placed in closed and pierced aluminum pans. The reference sample was an empty aluminum pan. An intracooler was used for cooling. For composite samples (POM/HAp-*g*-PEG), the measurement was carried out in a

dynamic mode, in which the sample was heated (25–200 °C), then cooled (200–25 °C), and reheated to 200 °C. On the basis of the obtained DSC curves, the enthalpy of melting (ΔH_m) of POM was determined, and then the degree of crystallinity of POM in POM/HAp-*g*-PEG composites was determined using the Equation (1):

$$X_c = \frac{\Delta H_m}{(1-w)\Delta H_m^0} \cdot 100\% \quad (1)$$

where X_c – degree of crystallinity of the POM, ΔH_m – heat of fusion of the sample, w – weight fraction of the additive (HAp-*g*-PEG) in the composite, ΔH_m^0 – heat of fusion of 100% crystalline polymer (X_c = 100%), for POM ΔH_m^0 =326.3 J/g. For the purpose of calculating the crystallization kinetics, isothermal measurements were also carried out, during which samples weighing about 5 mg were heated to a temperature of 180 °C, kept for 5 minutes until the polymer completely melted, and then rapidly cooled at a rate of 80 K/min to the crystallization temperature of POM.

Measurements using the dynamic mechanical analysis method were carried out using a DMA 850 Discovery (TA Instruments, USA) operating in the bending mode with the specimen fixed at one end (single cantilever). The measurements were carried out in a nitrogen atmosphere, in the temperature range of –90 to 150 °C, by heating the samples at a rate of 3 °C/min, deforming them at a frequency of 10 Hz with an amplitude of 10 μm. The dimensions of the samples for measurement are 20×4.75×4.05 mm. The atomic force microscope (AFM, XE120 Park Systems) was used to image the surface of the composites. Measurements were carried out in the contact mode, in the air atmosphere. A probe with a scanning blade (MLCT-C) by Bruker, made of non-conductive V-shaped silicon nitride, was used for the measurements. The measurement probe (MLCT-C) was characterized by the following parameters: resonant frequency 4–10 kHz. As a result of the measurements, images with dimensions of 90×90 μm, were obtained.

3. Results and discussion

Hybrid HAp-*g*-PEG systems were analyzed in the first stage of the investigation to assess the amount of organic phase in the systems – Figure 1.

For systems containing HDI as a coupling agent in their structure, a much higher proportion of the

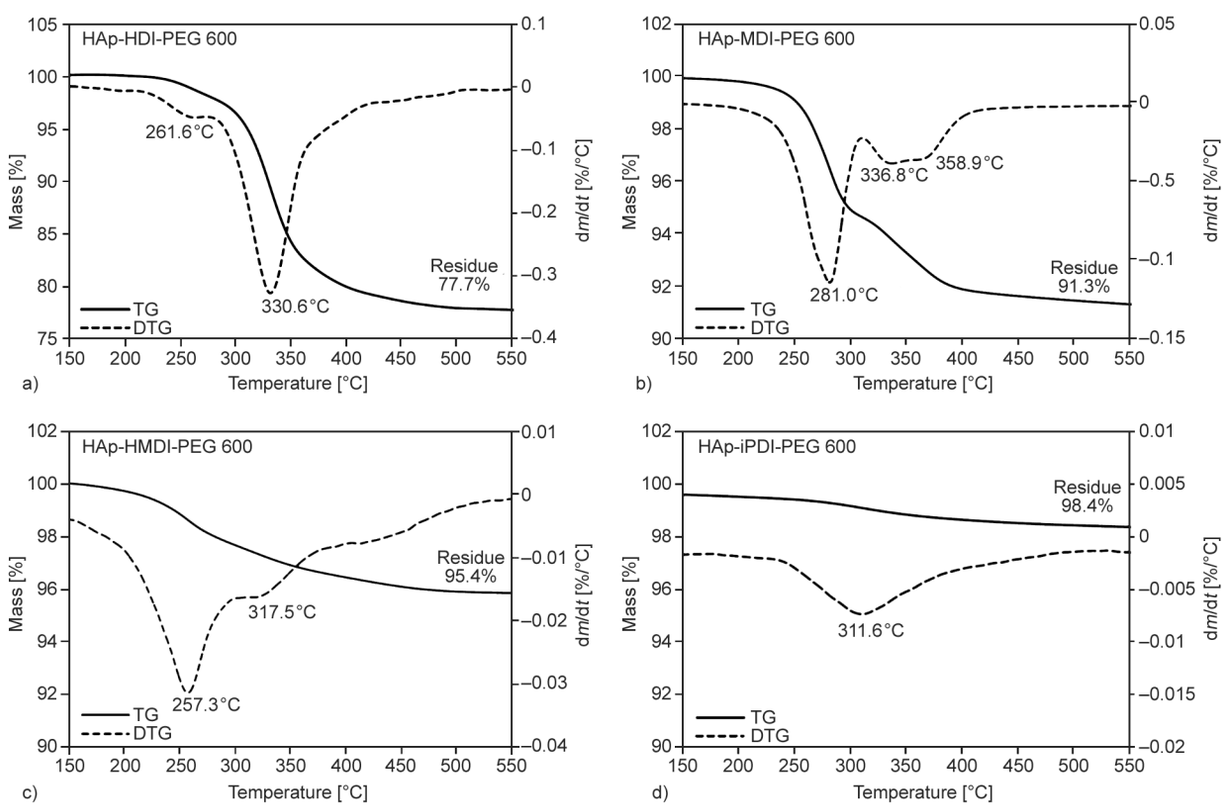

Figure 1. TG and derivative thermogravimetry (DTG) curves of hybrid HAp-*g*-PEG systems a) HAp-HDI-PEG 600, b) HAp-MDI-PEG 600, c) HAp-HMDI-PEG 600, d) HAp-iPDI-PEG 600.

organic phase (21.2±3.6%) than the other diisocyanates was observed. The degradation process of the organic part of HAp-*g*-PEG systems was carried out in three stages, which is confirmed by the presence of three peaks in the DTG curves. The onset of decomposition was around 210 °C. The first decomposition peak was observed at 250–280 °C, the second peak at 310–340 °C, and the third at 350–400 °C. The grafting reaction was unsuccessful for the system containing iPDI as the coupling agent. In the sample analyzed >98% of the inorganic phase (HAp) was present. For systems containing MDI and HMDI diisocyanates, the content of the incorporated organic phase did not exceed 10% of the sample weight.

The highest efficiency of the grafting reaction was obtained for HDI. The process of degradation of the organic part of the hybrid HAp-*g*-PEG system was similar to the degradation of polyurethanes obtained with polyethers as a soft segment, where the thermal decomposition of polyurethane (PU) hard segments (derived from the isocyanates used) at temperatures of 200 to 300 °C occurs as a result of the degradation of urethane bonds. The urethane bond can be degraded by dissociation to isocyanate and alcohol (re-formation of –NCO and –OH groups), or to primary amines (R–NH_2) and olefins (CH_2=C–R′) to form carbon dioxide (CO_2) and by eliminating CO_2 from the urethane bond to give secondary amines (R–NH–R′). After this stage, there was a further degradation of the material at temperatures of 355–385 °C, related to the degradation of soft segments derived from polyols. At this stage, the processes such as chain depolymerization, random chain breaking, and cross-linking take place. With further heating (>550 °C), complete decomposition of PU occurs with the formation of simple hydrocarbons and other residues [15, 16]. At temperatures up to 100 °C, HAp shows a slight weight loss (about 2%) [17] due to the release of absorbed water from the material; therefore, the solid residue at 550 °C is almost entirely composed of HAp.

The organic phase content in the HAp-*g*-PEG hybrid systems was also examined by means of elemental analysis of nitrogen, carbon, and hydrogen. The measurement results are presented in Table 2.

A much larger weight fraction of the examined elements was observed in the samples obtained with HDI. Among the elements examined, each of the samples contained the highest percentage by weight of C. In the sample obtained from iPDI, the presence of the elements N and H was not observed. The elemental analysis confirmed the presence of an organic phase in the HAp-*g*-PEG systems. The analysis results of the analysis coincide with the relationships obtained by the TG method, which indicates the highest efficiency of the syntheses performed with the use of HDI as a coupling agent and the lack of iPDI reactivity in a given system. The elemental analysis for the HAp-iPDI-PEG 600 sample indicates that the hydrogen comes only from the organic phase of the test compounds. The method does not detect hydrogen in HAp particles, whose weight ratio is 0.2%. The difference in the percentage of elements in the measurement compared to the TG analysis results from the lack of detection of a significant amount of oxygen atoms that make up the organic phase of the tested compounds.

Table 2. Elemental analysis results for HAp-*g*-PEG systems.

Sample	Elements [wt%]			
	N	C	H	Summa
HAp-HDI-PEG 600	2.10	13.72	1.97	17.78
HAp-HDI-PEG 2000	1.55	15.06	2.67	19.28
HAp-HDI-PEG 6000	1.62	10.89	1.86	14.37
HAp-MDI-PEG 600	0.38	7.31	0.50	8.18
HAp-HMDI-PEG 600	0.02	3.31	0.12	3.45
HAp-iPDI-PEG 600	0.00	1.62	0.00	1.62

In the next research stage of the research, NMR measurements of HAp-*g*-PEG powders were performed. The ^{31}P NMR spectra of all tested powders, the ^{13}C NMR spectra and ^{1}H NMR spectra for the powders with the highest organic phase content are presented in Figure 2.

For the ^{31}P NMR spectra of all powders tested, a single peak was visible, the maximum of which was 2.64 ppm, and its half-width was 2.07±0.02 ppm. This peak corresponds to the PO_4^{3-} phosphate groups present in the crystalline HAp; however, a slight chemical shift is observed in relation to the unmodified HAp for which the maximum from the PO_4^{3-} groups is 2.8 ppm [18]. The width of the peaks does not change much, while the intensity of the peaks obtained changes, which decreases in proportion to the increasing amount of the organic phase in HAp-*g*-PEG systems. These results are consistent with previous data from the TG analysis and elemental analysis of elements, in which the greatest share of this phase is present in systems containing HDI. In all the powders analyzed, the phosphorus environment is similar, which is related to the presence of

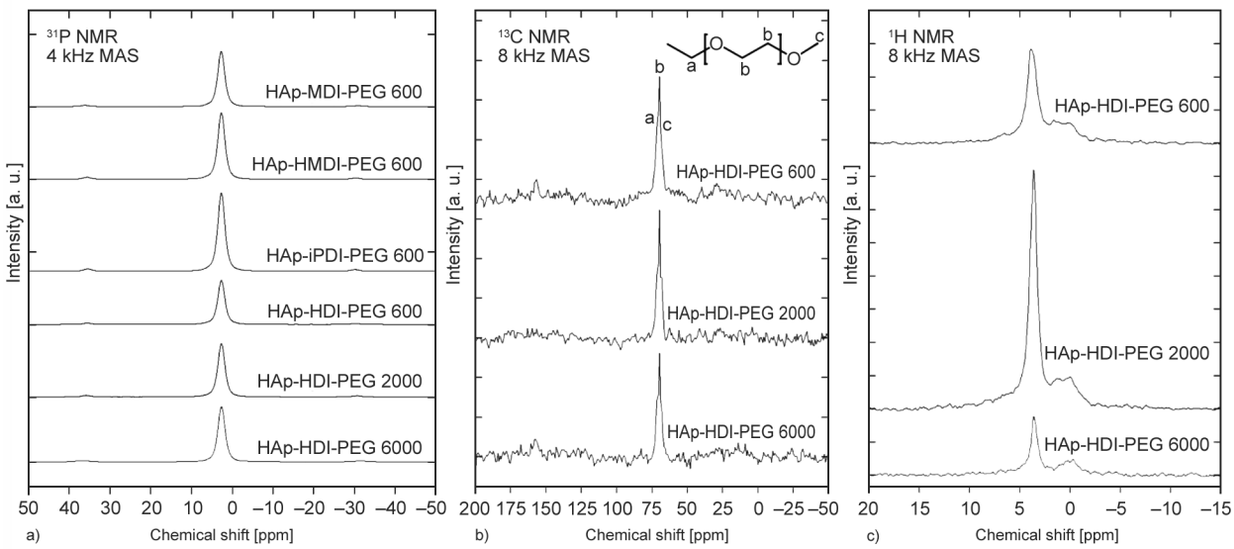

Figure 2. a) ^{31}P NMR, b) ^{13}C NMR, and c) ^{1}H NMR spectra of hybrid HAp-*g*-PEG systems.

the organic phase in the tested systems, which may affect the chemical shift compared to pure HAp. The lack of change in the half-width of the phosphate ions also proves that their crystal structure in HAp is preserved.

In the ^{13}C NMR spectra, there is a single asymmetric peak with a maximum at 69.7 ppm. The half-width is 3.56, 3.30, and 2.97 ppm, respectively, and decreases with increasing molar mass of PEG in the tested powders. This peak is from the PEG backbone ($–(CH_2–CH_2–O)_n–$) and consists of three adjacent C-derived peaks in the PEG chains. Furthermore, the spectra show weak peaks with a maximum of about 156.3 ppm due to the presence of carbon atoms in the urethane bond (–NH(C=O)O–) [19, 20]. NMR analysis confirmed the chemical structure of the compounds tested, in which both organic and inorganic parts are present. The obtained results agree with the TG analysis carried out earlier, confirming the different content of HAp in the tested systems. The dominant peak is visible in the ^{1}H NMR spectra, the maximum of which is 3.6 ppm (3,8 ppm for HAp-*g*-PEG 600) which corresponds to the H atoms in the PEG backbone ($–CH_2–CH_2–O–$), confirming thus the presence of this compound in the tested samples [21]. In addition, a much weaker double peak around 1.6–1.1 ppm is visible, corresponding to the hydrogen atoms in the chains derived from HDI (…$–CH_2–CH_2–CH_2–$…), the position of which shifts towards lower numbers as the molecular weight of poly(ethylene glycol) increases. The peak of hydrogen atoms near the urethane bond (NH–CO–O) should be visible around 3.0 ppm but is overlapped by the PEG peak [22]. Furthermore, around 5.5 ppm, weak peaks appear from hydrogen atoms derived from HAp, being components of hydroxyl groups and H_2O molecules associated in the structure of HAp [23].

Because of the highest efficiency of the syntheses performed with the use of HDI as a coupling agent, the next part of this work focused mainly on the systems obtained with the use of this diisocyanate. Studies were carried out for HAp-*g*-PEG X systems, where grafting was performed with HDI, and X was the average molecular weight of the PEG (X =600, 2000 or 6000).

TEM micrographs (Figure 3) show the distribution of the selected HAp-*g*-PEG systems in the POM_C matrix containing 1.0 and 5.0% of the additive. Hybrid HAp-*g*-PEG systems are visible in the form of interconnected HAp molecules embedded in the organic phase of the hybrid system made of HDI and PEG. Both HDI and PEG used for HAp-*g*-PEG preparation possess two functional groups, while on the surface of HAp nanoparticles there are more hydroxyl groups able to react with HDI. That probably leads to the formation of interconnections between HAp nanoparticles and agglomerates of HAp nanoparticles. The distribution of HAp-*g*-PEG agglomerates in the POM_C matrix is relatively uniform, even for composites containing 5.0% additive. It is contrary to the unmodified HAp in POM, which in the POM_C matrix was visible in the form of individual nanospheres or physically connected agglomerates containing up to several linked HAp nanoparticles [24, 25].

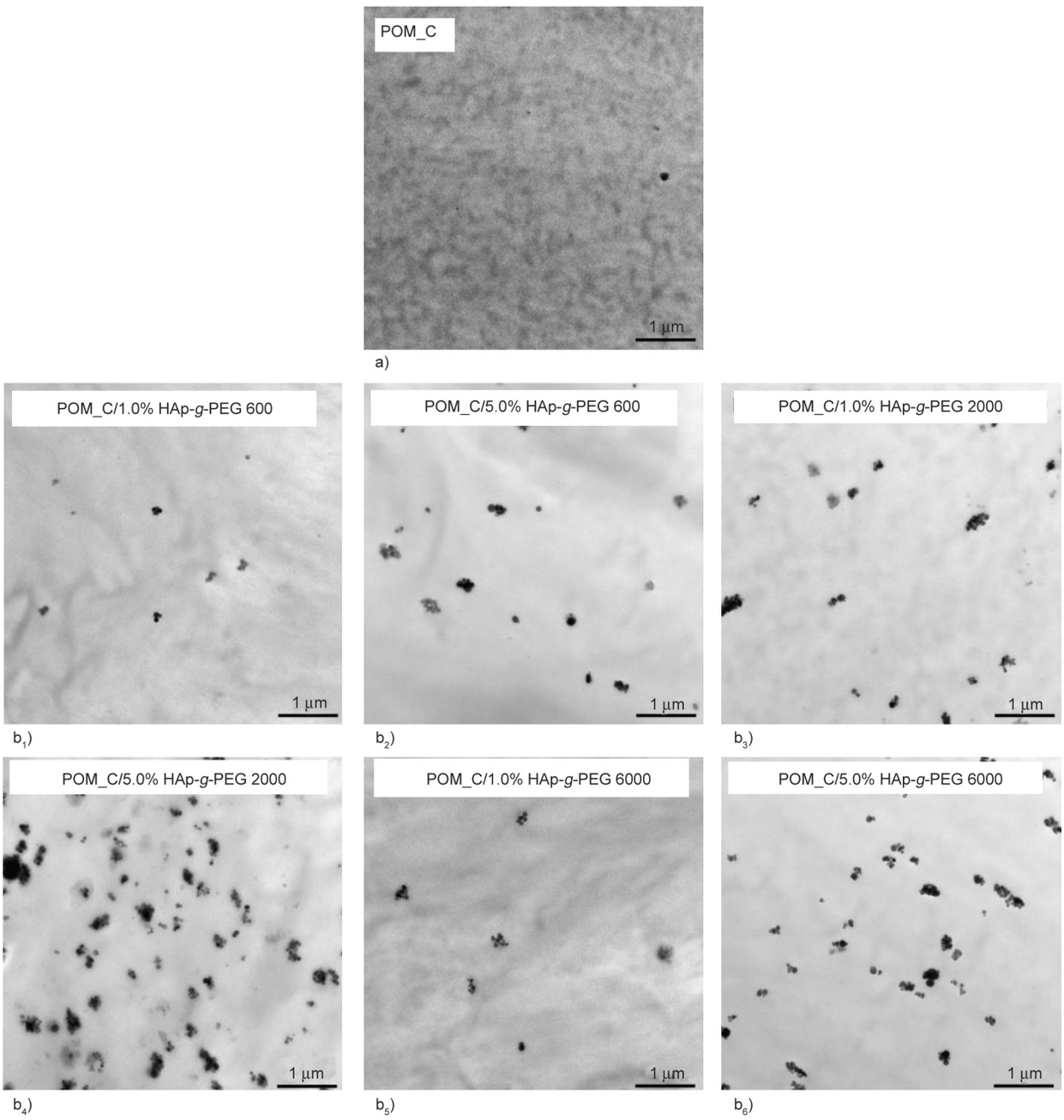

Figure 3. TEM micrographs of POM_C (a) and its composites with 1.0 and 5.0% load of HAp-*g*-PEG 600, HAp-*g*-PEG 2000, and HAp-*g*-PEG 6000 (b), (b_1) POM_C/1.0% HAp-g-PEG 600, b_2) POM_C/5.0% HAp-g-PEG 600, b_3) POM_C/1.0% HAp-g-PEG 2000, b_4) POM_C/5.0% HAp-g-PEG 2000, b_5) POM_C/1.0% HAp-g-PEG 6000, b_6) POM_C/5.0% HAp-g-PEG 6000.).

In the first stage, all the obtained POM/HAp-*g*-PEG composites were subjected to DSC analysis to determine the effect of the applied additive on the melting point, as it is one of the most important processing parameters. The measurement results are presented in Figure 4 and Table 3.

The addition of HAp-*g*-PEG insignificantly influenced the shape of the DSC curves, the melting point, and the degree of POM crystallinity in the composites. For samples containing a large amount of HAp-*g*-PEG (≥5%), the supercooling value was reduced even by 3 °C. In the second heating, the differences in melting point compared to unmodified POM did not exceed 1.6 °C. The degree of crystallinity calculated from the second melting increased by up to 5% , compared to the first heating. For the second heating, no major changes in the degree of POM crystallinity were observed (approximately 1–2% increase). The slight influence of the addition of HAp-*g*-PEG on the melting point of the

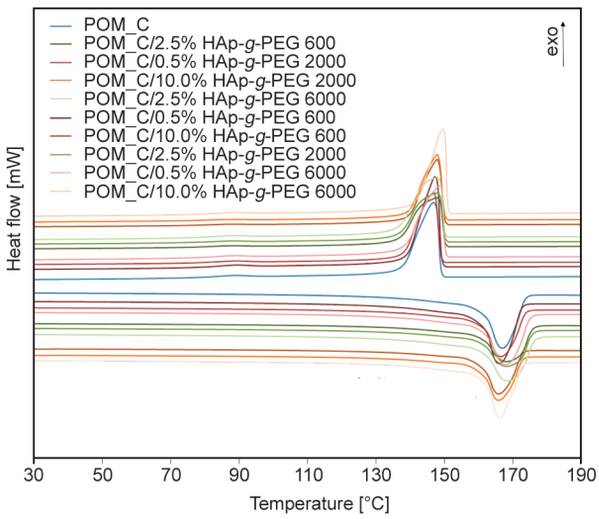

Figure 4. DSC curves (crystallization and melting, 2nd heating run) of POM_C and POM composites with HAp-*g*-PEG 600, with HAp-*g*-PEG 2000, and HAp-*g*-PEG 6000. Data for POM_C was taken from Ref. [26].

tested composites is important information because of the lack of necessity to change the processing conditions of the tested materials. No peak was observed in any of the DSC curves obtained, corresponding to the melting process of PEG, which are 17–22, 50–53, and 58–63 °C for PEG 600, 2000, and 6000, respectively [28]. The lack of peaks may suggest the chemical bonding of PEG in an inorganic-organic compound with HAp, which limits the mobility of the chains, and therefore they do not undergo the process of crystallization.

Contrary to the previously tested POM_C/HAp [25], no double peak in the 1st heating profile was observed, suggesting that the addition of HAp-*g*-PEG does not significantly affect the thickness variation of POM lamellae formed during the crystallization process. In contrast to unmodified HAp, where HAp nanopowder additionally induced the nucleation effect of POM crystals, no significant improvement in the degree of POM crystallinity was observed as a result of the presence of HAp-*g*-PEG. This may be due to too many HAp-*g*-PEG agglomerates linked by organic chains.

The presence of a double melting peak is probably related to the melting of the poorly formed POM_C crystals. Additionally, the presence of HAp-*g*-PEG may interfere with the POM_C crystallization process, especially with a high amount of additive. As a result, the intensity of the recrystallization phenomenon of imperfect POM_C crystals increases, which precedes further melting of better-formed POM_C crystals. A similar phenomenon was observed by Pielichowska *et al*. [29] for polyurethanes of MDI-PEG-BDO structure modified with nanographite. In the next stage, the samples were subjected to spectroscopic examination. The FTIR-ATR spectra and their second derivative are shown in Figure 5. In the analyzed spectra, there is a group of two bands: 2981 and 2923 cm^{-1}, which were not included in the figures, corresponding to the symmetrical stretching vibrations (ν) of the CH_2 groups. The band visible at about 1475 cm^{-1} is related to the bending vibrations (δ) of the CH_2 groups. The band at about 1393 cm^{-1} was created as a result of the wagging vibrations of the CH_2 groups, while the average size band at about 1236 cm^{-1} is the effect of the torsional vibrations of the CH_2 groups. The two strong bands at 1093 and 895 cm^{-1} and the weaker band at 1139 cm^{-1} are the results of asymmetric stretching vibrations, and the band at 929 cm^{-1} is caused by symmetric stretching vibrations of the C–O–C bonds. Moreover, at 630 cm^{-1} a peak appears that is related to the bending vibrations of C–O–C bonds [31]. For samples containing at least 2.5% HAp-*g*-PEG addition, two bands (607 and 578 cm^{-1}) are visible, resulting from asymmetric bending vibrations of PO_4^{3-} phosphate ions derived from HAp.

As is known, POM most often crystallizes in the hexagonal system, in which the polymer chains exist in a 9/5 helical conformation. Only under specific conditions do POM chains in the 2/1 spiral form crystallize in the orthorhombic system to form metastable crystals. In the classic hexagonal arrangement, POM chains crystallize in both an extended and a folded form. Although IR spectroscopy is one of the few methods that can distinguish the bands from each type of crystal produced, it is relatively difficult to separate the peaks from each of them. According to data presented in the literature [32], only two bands are characteristic of one type of POM crystals. These are the band at 1136 cm^{-1}, coming only from the vibrations of the FCC crystals, and the band at 891 cm^{-1}, which is the result of vibrations of the ECC crystals. The remaining bands (1236, 1089, 933, 630 cm^{-1}) result from the superposition of vibrations of both the ECC and FCC crystals. No changes in the values and the number of peaks in POM/HAp-*g*-PEG composites indicate that, similarly to unmodified POM, crystals in the form of ECC and FCC are also present in these materials.

Table 3. Temperature and heat of fusion or crystallization of POM_C and composites. POM_C/HAp-*g*-PEG 600, POM_C/HAp-*g*-PEG 2000 and POM_C/HAp-*g*-PEG 6000*

Sample	T_{onset} [°C]	T_{max} [°C]	T_{endset} [°C]	Heat of melting POM_C/HAp-*g*-PEG [J/g]	Degree pf crystallinity [%]
HAp-*g*-PEG 600					
Melting					
POM_C_0%	160	167	174	171	52.4
POM_C_0,5%	160	166	173	173	53.2
POM_C_1%	160	168	175	167	51.6
POM_C_2,5%	160	169	176	172	54.1
POM_C_5%	160	167	174	160	51.7
POM_C_10%	160	165	174	157	53.0
Crystallization					
POM_C_0%	149	147	137	168	
POM_C_0,5%	149	147	139	171	
POM_C_1%	149	147	137	168	
POM_C_2,5%	150	147	136	170	
POM_C_5%	150	148	139	161	
POM_C_10%	151	149	139	155	
HAp-*g*-PEG 2000					
Melting					
POM_C_0%	160	167	174	171	52.4
POM_C_0,5%	160	166	174	167	51.5
POM_C_1%	160	167	174	170	52.6
POM_C_2,5%	160	168	176	170	53.5
POM_C_5%	160	166	174	165	53.4
POM_C_10%	160	166	173	159	54.0
Crystallization					
POM_C_0%	149	147	137	168	
POM_C_0,5%	149	147	138	172	
POM_C_1%	150	147	138	170	
POM_C_2,5%	150	148	137	169	
POM_C_5%	150	148	139	164	
POM_C_10%	150	148	140	155	
HAp-*g*-PEG 6000					
Melting					
POM_C_0%	160	167	174	171	52.4
POM_C_0,5%	160	168	175	169	52.0
POM_C_1%	160	166	172	172	53.2
POM_C_2,5%	160	169	176	169	53.1
POM_C_5%	160	168	176	160	51.7
POM_C_10%	160	167	173	153	52.2
Crystallization					
POM_C_0%	149	147	137	168	
POM_C_0,5%	150	149	138	168	
POM_C_1%	151	149	141	172	
POM_C_2,5%	150	148	136	168	
POM_C_5%	150	148	137	159	
POM_C_10%	151	150	142	156	

*Data for POM_C, POM_C_1% and POM_C_5% were taken from Ref. [27].

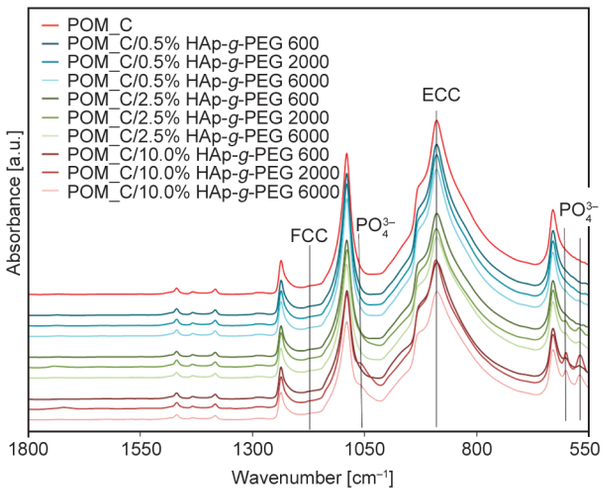

Figure 5. FTIR-ATR spectra of unmodified POM_C and composite spectra POM_C with HAp-*g*-PEG 600, HAp-*g*-PEG 2000, and HAp-*g*-PEG 6000. Data for POM_C were taken from Ref. [30]

In the next stage of the research, the analysis by ^{31}P NMR and ^{13}C NMR methods was carried out for POM_C and its composites with 1.0 and 5.0% HAp-*g*-PEG 600, HAp-*g*-PEG 2000 and HAp-*g*-PEG 6000. Due to the lack of phosphorus atoms in the samples of the unmodified POM, the ^{31}P NMR analysis was not performed for the pristine polymer. The results of both measurements are presented in Figure 6.

On the ^{31}P NMR spectra for each of the composites tested, a symmetric peak with a constant position of 2.52 ppm and a half-width of 2.10±0.06 ppm was visible, which differed in intensity for various contents of HAp-*g*-PEG, which confirms the different amount of HAp in the tested samples. In the ^{13}C NMR spectra, an asymmetric peak is visible, the maximum of which is 88.31 ppm, which is characteristic of the carbon atoms in the main chain of the polyacetal –[CH_2–O]$_n$– forming the crystalline phase [33]. Additionally, the broadening of each of the peaks at the bottom left is visible with an additional shoulder that corresponds to the POM carbon atoms in the amorphous phase [34]. The half-width of the observed peak is 5.5±0.2 ppm, and there is a slight effect of the addition of HAp-*g*-PEG on the half-width of the analysed peak. Moreover, for the sample containing 5.0% HAp-*g*-PEG 2000, the spectrum shows a second peak with a maximum of 69.6 ppm, corresponding to the carbon atoms environment due to the addition of HAp-*g*-PEG 2000.

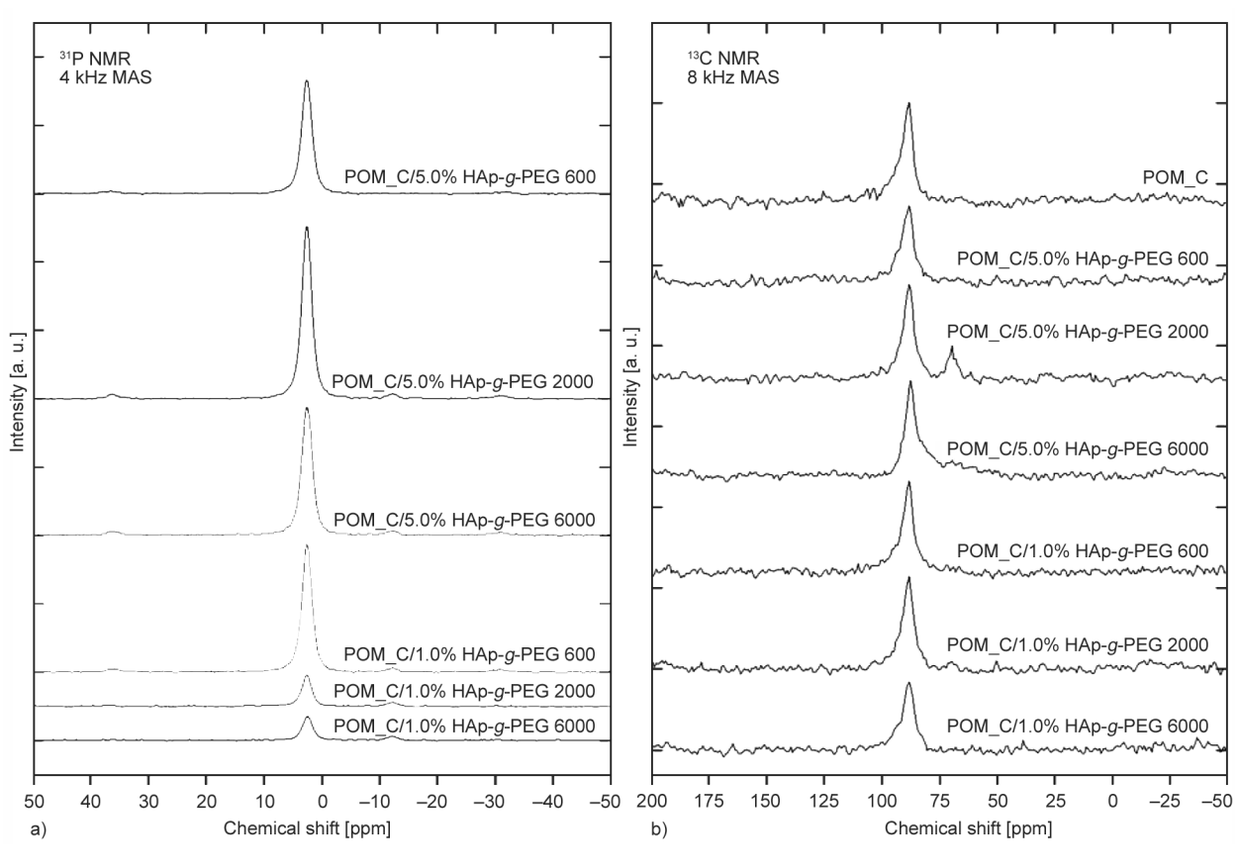

Figure 6. ^{31}P NMR (a) and ^{13}C NMR (b) spectra for POM_C and POM_C composites with 1.0 and 5.0% HAp-*g*-PEG 600, HAp-*g*-PEG 2000, and HAp-*g*-PEG 6000.

NMR tests confirmed the presence of various amounts of HAp in the tested samples. A clear chemical shift for PO_4^{3-} ions compared to unmodified HAp may indicate the presence of an inoculated organic phase. Moreover, NMR analysis revealed the semicrystalline nature of POM_C. However, the addition of HAp-*g*-PEG did not change the structure of the POM_C chains, as it was confirmed by the XRD analysis performed earlier [26].

For POM_C samples and their composites containing 1.0 and 5.0% of HAp-*g*-PEG 600, HAp-*g*-PEG 2000, and HAp-*g*-PEG 6000, measurements were carried out using a DSC to analyze the kinetics of crystallization. After crystallization of the samples under isothermal conditions at four selected temperatures, the obtained DSC curves were subjected to integration to determine the relative degree of crystallinity, or (X_t), according to Equation (2):

$$X_t = \frac{\int_0^t \frac{dH}{dt} dt}{\int_0^\infty \frac{dH}{dt} dt} \quad (2)$$

where X_t – relative crystallinity, dH/dt – heat flux of accompanying the transformation.

The curves of the dependence of the degree of relative crystallinity X_t on the crystallization time t obtained in this way for selected samples are presented in Figure 7.

As can be seen from the analyzed curves, the higher the temperature of the crystallization, the longer its time. The characteristic sigmoidal shape of the obtained curves, for which a rapid increase in the rate of crystallization takes place in the first stage, is related to the occurrence of the so-called primary crystallization, which precedes secondary crystallization taking place much more slowly. After the primary crystallization is completed, secondary crystallization begins, which includes the further process of organizing the amorphous areas remaining in the polymer [35]. The kinetics of primary crystallization of a number of polymers, including POM, under isothermal conditions can be described using the Avrami Equation (3):

$$X_t = 1 - \exp(-kt^n) \quad (3)$$

where X_t – the relative degree of crystallinity achieved by the polymer that crystallizes over time t, k – Avrami constant, the isothermal crystallization rate constant depending on the nucleation frequency and spherulite growth rate, n – Avrami exponent, depending on the nucleation mechanism and shape of growing crystallites [36].

The doubly logarithmic form of the Avrami equation is used to determine the parameters n and k (Equation (4)):

$$\log[-\ln(1 - X_t)] = \log k + n \log t \quad (4)$$

From the dependency graph $\log[-\ln(1 - X_t)]$ *vs.* $\log t$ – for selected samples shown in Figure 8, the Avrami exponent n and the constant k were determined from the straight line equation.

By knowing the value of the Avrami constant (k), the half-time of crystallization was determined using Equation (5):

$$t_{1/2} = \left(\frac{\ln 2}{5}\right)^{\frac{1}{2}} \quad (5)$$

where $t_{1/2}$ – half-time crystallization, that is the time taken to reach the relative degree of crystallinity of 50% and the rate of crystallization as reciprocal of the half time (G) based on the Equation (6):

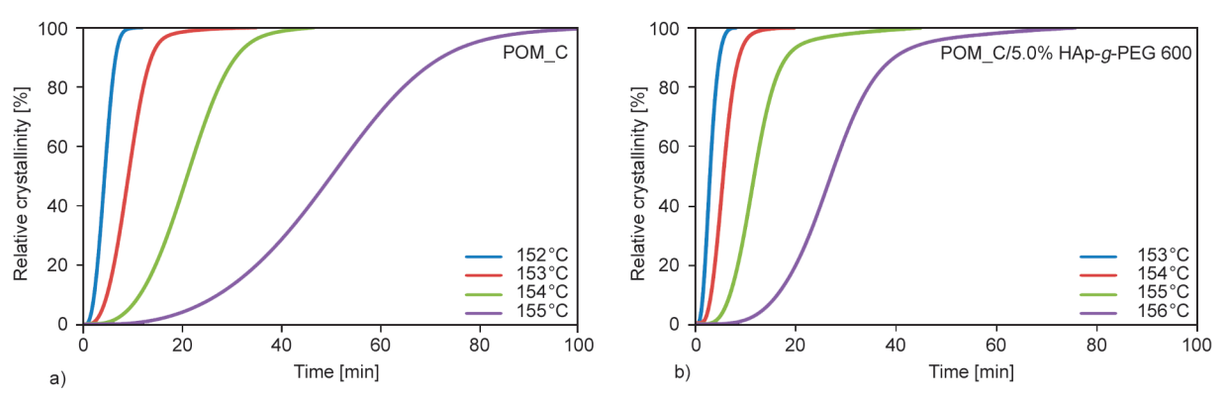

Figure 7. Relative crystallinity (X_t) *vs.* time (t) for isothermal crystallization process of a) POM_C and b) POM_C composites with 5.0% HAp-*g*-PEG 600.

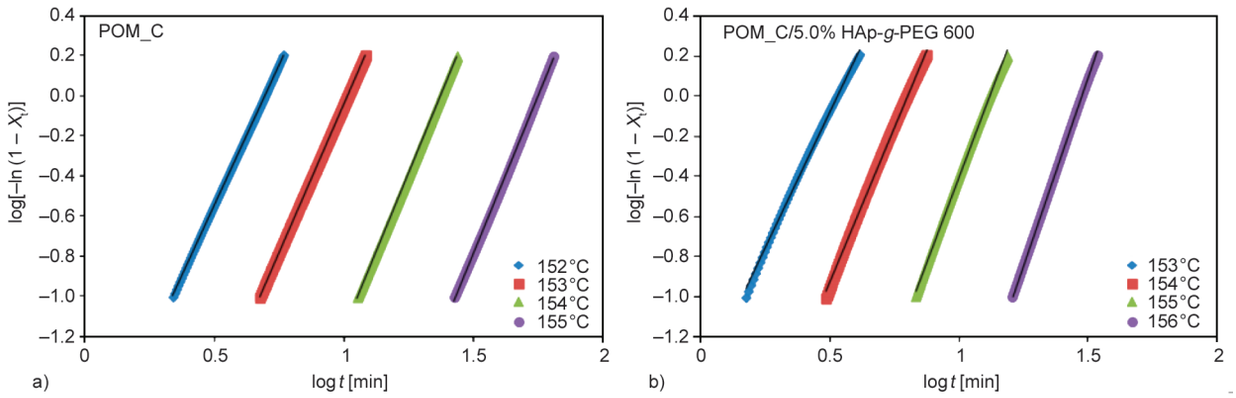

Figure 8. $\log[-\ln(1-X_t)]$ *vs.* $\log t$ for isothermal crystallization process of a) POM_C and b) POM_C composites with 5.0% HAp-*g*-PEG 600.

$$G = \frac{1}{t_{1/2}} \tag{6}$$

The time required to reach the maximum crystallization rate (t_{max}) can be calculated from Equation (7):

$$t_{max} = \left(\frac{n-1}{nk}\right)^{\frac{1}{n}} \tag{7}$$

The values of the parameters determined n, k, $t_{1/2}$, G, t_{max} including isothermal crystallization temperatures (T_K) and the R^2 coefficient, are summarized in Table 4.

For POM_C composites containing 1.0% additive HAp-*g*-PEG 600, HAp-*g*-PEG 2000, and HAp-*g*-PEG 6000 at 153 °C, compared to unmodified POM_C, there was a significant acceleration of crystallization (t_{max}) by 46, 52, and 62%, respectively. For all composites containing 5.0% HAp-*g*-PEG, crystallization at 153 °C was accelerated by 67.6±0.7%. This indicates accelerated crystallization as a result of the presence of HAp-*g*-PEG, which may constitute nuclei for POM, thus supporting the heterogeneous nucleation process of this polymer [37]. With a small proportion of HAp-*g*-PEG addition (1.0%), the greater the average molar mass of PEG in the HAp-*g*-PEG, the more enhanced the crystallization acceleration effect, while with a higher amount of additive (5.0%), all additives work in a similar manner. The value of the Avrami exponent for unmodified POM_C ranges from 2.80 (at 152 °C) to 3.16 (at 155 °C), indicating the formation – under given conditions – of three-dimensional POM crystal structures in the form of spherulites [38]. Data from the literature show that for the value of the Avrami exponent $n = 3$, there is a two-dimensional growth of crystallites formed as a result of thermal nucleation and a three-dimensional growth of spherulites formed through thermal nucleation [38]. For most of the POM/HAp-*g*-PEG composites, the Avrami exponent (n) slightly decreased by 0.1 to approx. 0.5, with the greatest reduction of n occurring mainly in the composites containing 5.0% of HAp-*g*-PEG.

The reduction of the n value of the tested composites may indicate that the presence of HAp-*g*-PEG, especially in a larger amount, may hinder the formation of three-dimensional spherulites during POM crystallization. Polymer chains can crystallize in a two-dimensional form, in the form of lamellas arranged in flat disks [39]. The value of the constant k decreases with the increasing crystallization temperature for both pure POM_C and its composites. This is because the difference between the temperature at which crystallization is carried out and the temperature corresponding to the highest crystallization rate increases. In composite materials, the k value is significantly greater than the k value for pure POM_C at the corresponding crystallization temperatures. At the same time, the increase in k value is much greater for composites containing 5.0% HAp-*g*-PEG. Analogous dependencies exist for the parameter G, which is the reciprocal of the half-time of crystallization. A similar relationship was noticed by Xu [40] when studying POM with attapulgite, which was used as a nucleating agent. The addition of attapulgite reduced the size of POM spherulites, significantly accelerated the rate of crystallization, and improved impact toughness, but did not affect the hexagonal form of the crystallizing POM, similarly to the HAp-*g*-PEG additives used in our study.

Figure 9 shows the rate of crystallization (G) described as the reciprocal of the half-time, which determines the crystallization rate *vs.* isothermal

Table 4. Values of the kinetic parameters of the crystallization process obtained from the Avrami equation for POM_C and composites with 1.0 and 5.0% HAp-*g*-PEG 600, HAp-*g*-PEG 2000, HAp-*g*-PEG 6000.

Sample	T_K [°C]	n	k [min^{-1}]	R^2	t_{max} [min]	$t_{1/2}$ [min]	G [min^{-1}]
POM_C	152	2.80	$1.16 \cdot 10^{-2}$	1.0000	4.20	4.31	0.2320
	153	2.94	$1.04 \cdot 10^{-3}$	1.0000	8.96	9.11	0.1098
	154	3.13	$5.12 \cdot 10^{-5}$	0.9999	20.84	20.97	0.0477
	155	3.16	$3.00 \cdot 10^{-6}$	0.9995	49.71	49.93	0.0200
POM_C/1.0% HAp-*g*-PEG 600	153	2.69	$9.22 \cdot 10^{-3}$	0.9997	4.80	4.98	0.2006
	154	2.90	$8.25 \cdot 10^{-4}$	0.9996	9.98	10.17	0.0983
	155	3.05	$4.85 \cdot 10^{-5}$	0.9993	23.20	23.44	0.0427
	156	3.25	$1.32 \cdot 10^{-6}$	0.9999	57.75	57.78	0.0173
POM_C/5.0% HAp-*g*-PEG 600	153	2.72	$3.64 \cdot 10^{-2}$	0.9976	2.86	2.96	0.3380
	154	3.11	$3.21 \cdot 10^{-3}$	0.9985	5.58	5.62	0.1781
	155	3.40	$1.55 \cdot 10^{-4}$	0.9987	11.88	11.82	0.0846
	156	3.71	$3.38 \cdot 10^{-6}$	0.9997	27.52	27.14	0.0368
POM_C/1.0% HAp-*g*-PEG 2000	153	2.60	$1.62 \cdot 10^{-2}$	0.9988	4.05	4.23	0.2262
	154	2.58	$2.99 \cdot 10^{-3}$	0.9994	7.85	8.23	0.1214
	155	2.71	$2.09 \cdot 10^{-4}$	0.9992	19.28	19.97	0.0501
	156	2.58	$2.59 \cdot 10^{-5}$	0.9964	49.81	52.28	0.0191
POM_C/5.0% HAp-*g*-PEG 2000	153	2.41	$4.65 \cdot 10^{-2}$	0.9992	2.86	3.07	0.3256
	154	2.69	$4.05 \cdot 10^{-3}$	0.9991	6.51	6.75	0.1481
	155	2.78	$3.19 \cdot 10^{-4}$	0.9998	15.44	15.89	0.0629
	156	2.85	$1.18 \cdot 10^{-5}$	0.9998	46.17	47.26	0.0212
POM_C/1.0% HAp-*g*-PEG 6000	153	2.71	$2.27 \cdot 10^{-2}$	0.9988	3.41	3.53	0.2833
	154	3.08	$1.64 \cdot 10^{-3}$	0.9993	7.07	7.13	0.1403
	155	3.27	$9.08 \cdot 10^{-5}$	0.9996	15.35	15.34	0.0652
	156	3.49	$2.42 \cdot 10^{-6}$	0.9998	36.88	36.57	0.0273
POM_C/5.0% HAp-*g*-PEG 6000	153	2.48	$3.97 \cdot 10^{-2}$	0.9989	2.98	3.17	0.3153
	154	2.69	$5.39 \cdot 10^{-3}$	0.9987	5.87	6.09	0.1642
	155	2.85	$4.29 \cdot 10^{-4}$	0.9978	13.07	13.37	0.0748
	156	3.01	$2.12 \cdot 10^{-5}$	0.9984	31.14	31.53	0.0317

crystallization temperature of POM_C and POM_C composites with 1.0 and 5.0% HAp-*g*-PEG 600, HAp-*g*-PEG 2000, and HAp-*g*-PEG 6000.

The presented dependencies confirm the increase in the rate of POM_C crystallization with the increase in the concentration of HAp-*g*-PEG addition. Based on Hoffman-Week diagrams, the equilibrium melting point T_m^0 for pure POM_C was 189 °C, and it decreases with increasing content of HAp-*g*-PEG as it was presented in Table 5. A larger decrease in T_m^0 was also observed with an increase in the average molar mass of PEG in the additive used. The drop in the equilibrium melting point indicates the formation of less developed and more defective POM_C crystals in the presence of HAp-*g*-PEG, the presence of which most likely disturbed the polymer crystallization process as a result of an increased share of heterogeneous POM_C nucleation in composites. The increased proportion of additional nucleation seeds in the polymer can result in the formation of smaller, more defective POM_C crystals, in this case, three-dimensional spherulites. A similar phenomenon was observed by Wu and Chen [41] when investigating PCL/MWCNT composites, where, also with the increase in the amount of additive, the temperature T_m^0 was decreased, and consequently, the microstructure of the composites changed by forming much smaller and less perfect PCL spherulites. Another explanation for the reduction of the equilibrium temperature T_m^0 is a significant reduction in the duration of crystallization as a result of heterogeneous POM_C nucleation on the surfaces of HAp-*g*-PEG particles, which reduces the time for the formation of polymer crystallites [42].

Depression of equilibrium melting point was described in the literature for many polymeric systems, especially for blends, but also for (nano)composites, and it is connected to the interactions between

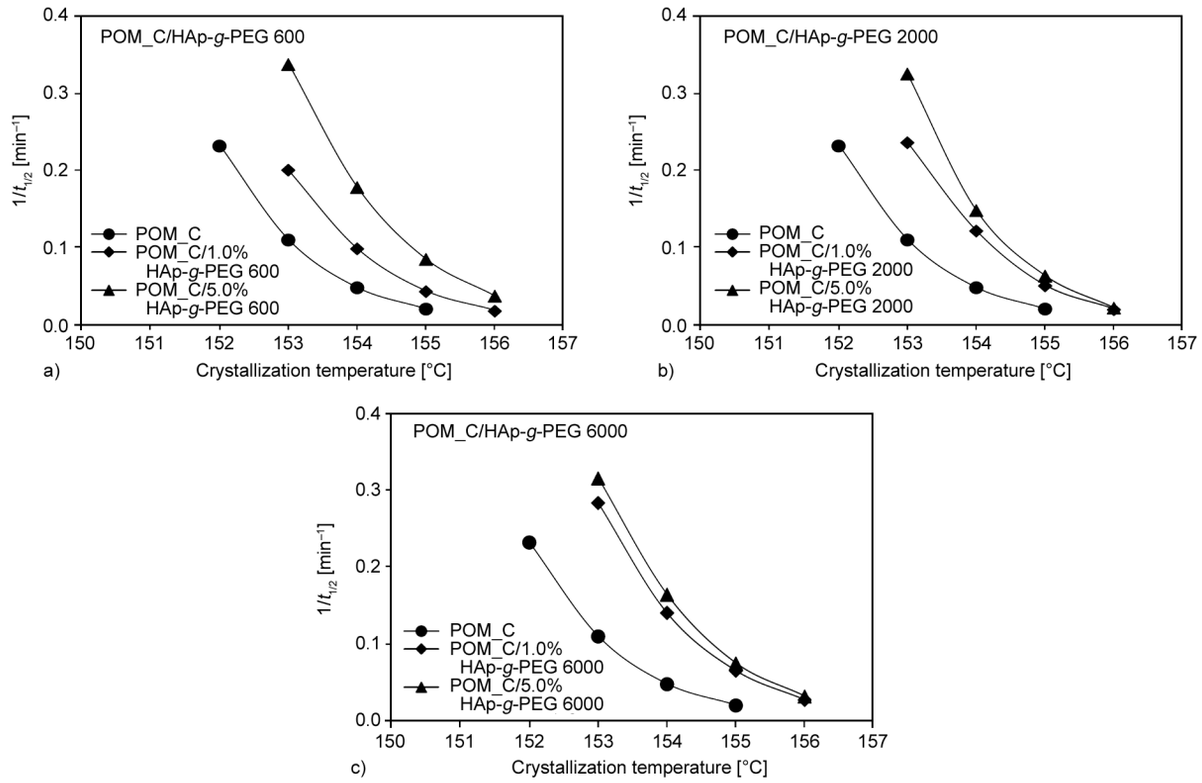

Figure 9. Plots of the reciprocal of the half-time (G) vs isothermal crystallization temperature (T_K) for POM_C and POM_C composites with 1.0 and 5.0% HAp-*g*-PEG 600 (a), HAp-*g*-PEG 2000 (b) and HAp-*g*-PEG 6000 (c).

components of the system and their miscibility [43] Depression of equilibrium melting point was analysed by Lee *et al*. [44] as a measure of interactions between PLA and MWCNTs.

The effective activation energy (E) was determined on the basis of Hoffman-Lauritzen theory using Equation (8):

$$E = a \cdot \frac{\mathrm{d}(\ln G)}{\mathrm{d}T^{-1}} = \\ = U\frac{T_K^2}{\left(T_K - T_\infty\right)^2} + K_g R\frac{\left(T_m^0\right)^2 - T_K^2 - T_m^0 T_K}{\left(T_m^0 - T_K\right)^2 T_K} \quad (8)$$

where E depends on the parameters U^* and K_g, which represent the energy barriers of mass transport and nucleation, respectively. In the assumed model, the linear growth rate of the polymer crystals (G) depends on the temperature, according to the Equation (9):

$$G = G_0 \exp\left[\frac{-U^*}{R(T_K - T_\infty)}\right]\exp\left[\frac{-K_g}{T_K \cdot \Delta T \cdot f}\right] \quad (9)$$

where G_0 – it is a pre-exponential factor, U^* – the activation energy necessary to initiate crystallization (for polymers, U^* has a constant value of 6.3 kJ/mol), R – universal gas constant, $\Delta T = T_m^0 - T_K$ and this is supercooling, $f = 2T_K/(T_m^0 + T_K)$ – correction factor, T_∞ – temperature of crystallization decay ($T_\infty = T_g - 30$ K, where T_g – polymer glass transition temperature).

The kinetic parameter K_g denotes the energy barrier for the nucleation of crystals of a critical size. K_g is strongly dependent on the degree of supercooling and can be calculated by Equation (10):

$$K_g = \frac{nb\sigma\sigma_e T_m^0}{\Delta h_f^0 k_B} \quad (10)$$

where b – thickness of the crystallite growth surface (b =4.46·10^{-10} m), σ – is the lateral surface free energy (σ = 0.0147 J/m^2), σ_e – is the fold surface free energy, Δh_f^0 – is the heat of fusion per unit volume of crystal (Δh_f^0 =3.55·10^8 Jm^{-3}), k_B – Boltzman's constant, n takes a value depending on the crystallization regime in a given system, for I and III regimes n = 4, for II regime n = 2 [45].

Taking the logarithm of Equation (9), the Equation (11) was obtained:

$$\log G + \left[\frac{-U^*}{R(T_K - T_\infty)}\right] = \log G_0 - \frac{-K_g}{T_K \cdot \Delta T \cdot f} \quad (11)$$

which can also be used to determine the parameter K_g. This parameter is determined from the linear relationship $\log G + U^*/[(R(T_K - T_\infty)]$ *vs*. $1/(T_K \cdot \Delta T \cdot f)$.

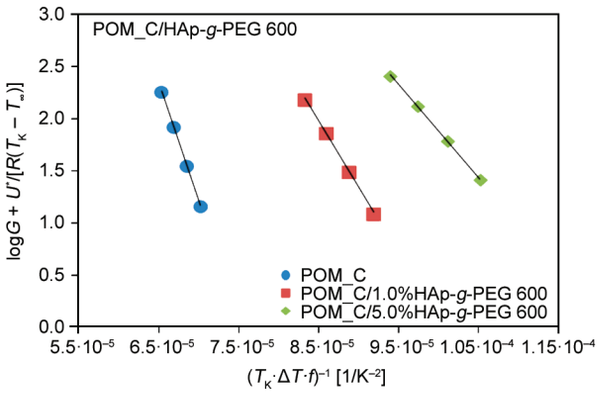

Figure 10. $\log G + U^*/[R(T_K - T_\infty)]$ *vs.* $1/(T_K \cdot \Delta T \cdot f)$ for POM_C and POM_C composites with 1.0 and 5.0% HAp-*g*-PEG 600.

This relationship for POM_C/HAp-*g*-PEG 600 is shown in Figure 10. The K_g values were read as the slope of the regression line fitted to the measuring points.

In Figure 10, a decrease in the degree of slope of the straight lines is visible with an increase in the content of the HAp-*g*-PEG additive. This, in turn, corresponds to a significant reduction of the energy barrier of crystal nucleation (K_g) in POM_C/HAp-*g*-PEG composites. Knowing the value of K_g and transforming the relationship in Equation (9), the amount of free energy was determined from the fold surface free energy of crystallites (σ_e). To determine the value of σ_e, the presence of the III crystallization regime was assumed in the materials tested, therefore the value of the parameter $n = 4$ was assumed. The determined K_g and σ_e values are summarized in Table 5.

Both values decreased with an increase in the HAp-*g*-PEG content and with an increase in the average molar mass of PEG in the addition of HAp-*g*-PEG. The process of forming polymer crystals on the surface of alien inclusions (in this case, HAp-*g*-PEG) requires less energy input than for the production of a sufficiently large homogeneous nucleus from the polymer chain, from which the crystal could be formed. Consequently, as the content of HAp-*g*-PEG increases, the material's surface, on which nucleation and formation of polymer crystals can occur, increases [46].

The last calculated parameter was the thickness of the lamella formed during crystallization L [nm], which was determined from the Gibbs-Thomson Equation (12) at 153 °C – Table 5.

$$T_m = T_m^0\left(1 - \frac{2\sigma_e}{\Delta h_0 L}\right) \tag{12}$$

where T_m – the melting point of POM after isothermal crystallization at 153 °C, T_m^0 – equilibrium melting point, Δh_0 – thermodynamic enthalpy of change per unit volume of the crystalline phase, σ_e – is the fold surface free energy of the lamellae, related to the crystallization process.

For pure POM_C, the average thickness of the formed lamellae was about 10.2 nm. The addition of HAp-*g*-PEG influenced the average value of the thickness of the lamellas by reducing it. The largest decrease was recorded for the POM_C/5.0% HAp-*g*-PEG 600 sample. The thickness of the lamellae depended on the equilibrium value of the melting point and the fold surface free energy of the lamellae formed, and it decreased as both values decreased.

In the next stage of the investigation, selected samples based on POM_C were melted and then placed at a temperature of 153 °C in order to carry out slow crystallization. The surface of the tested samples was observed using the SEM and AFM microscopic techniques to verify the resulting POM_C crystal structures. The results of the observations are presented in Figure 11.

The observations show that POM_C, both in its pure form and as a matrix for composites, crystallized in the form of spherulites, which, in contact with each other, filled the entire surface of the sample. This

Table 5. K_g, T_m^0, σ_e and L determined for POM_C and POM_C composites with 1.0 and 5.0% HAp-*g*-PEG 600, HAp-*g*-PEG 2000 and HAp-*g*-PEG 6000.

Sample	$K_g \cdot 10^5$ [K^2]	T_m^0 [K]	σ_e [J/m^2]	L at 153 °C [nm]
POM_C	2.24	463	0.0866	10.2
POM_C/1.0% HAp-*g*-PEG 600	1.28	455	0.0503	9.3
POM_C/5.0% HAp-*g*-PEG 600	0.88	452	0.0350	8.6
POM_C/1.0% HAp-*g*-PEG 2000	1.27	455	0.0495	9.3
POM_C/5.0% HAp-*g*-PEG 2000	1.14	453	0.0451	9.9
POM_C/1.0% HAp-*g*-PEG 6000	1.05	453	0.0415	9.1
POM_C/5.0% HAp-*g*-PEG 6000	0.84	451	0.0334	9.5

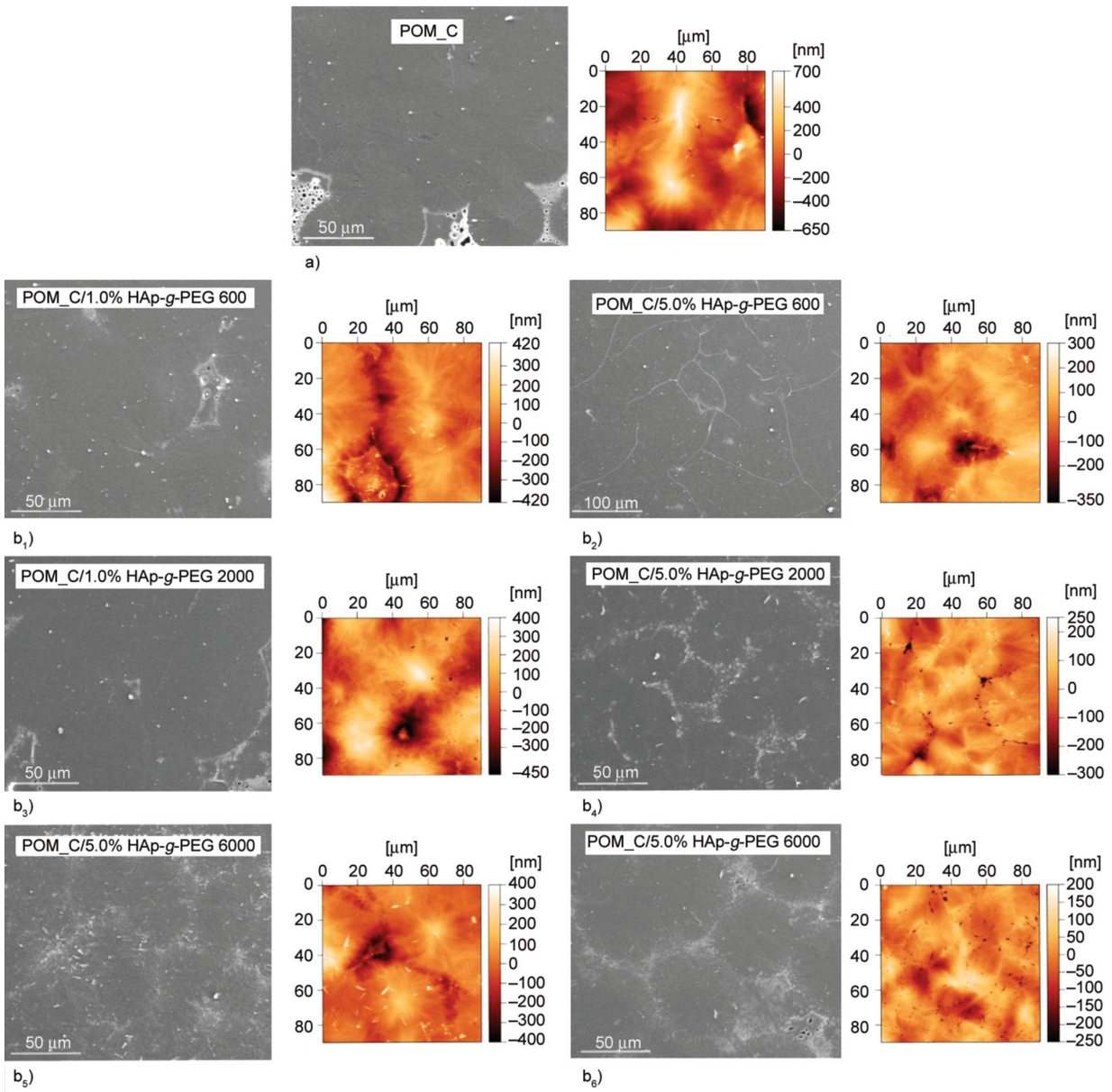

Figure 11. SEM and AFM images of a) POM_C surfaces and b) POM_C composites with 1.0 and 5.0% HAp-*g*-PEG, b_1) POM_C/1.0% HAp-*g*-PEG 600, b_2) POM_C/5.0% HAp-*g*-PEG 600, b_3) POM_C/1.0% HAp-*g*-PEG 2000, b_4) POM_C/1.0% HAp-*g*-PEG 2000, b_5) POM_C/1.0% HAp-*g*-PEG 6000, b_6) POM_C/1.0% HAp-*g*-PEG 6000.

result is consistent with the results of kinetic calculations, where the value of the Avrami exponent indicated just such a crystalline form of POM_C. With the 1.0% HAp-*g*-PEG addition, the size and shape of the spherulites are similar to those of the unmodified POM_C. On the other hand, for an increased amount of additive (5.0%), the spherulites are reduced and distorted; it is much more difficult to distinguish the boundaries between them. The increased amount of HAp-*g*-PEG addition may hinder the formation of POM_C three-dimensional crystal structures, which was also confirmed in the crystallization kinetics studies, where the Avrami exponent decreased with an increase in the HAp-*g*-PEG content.

Then, DMA tests were carried out for POM_C and selected composite samples in order to determine the glass transition temperature. The results of the DMA tests are presented in Figure 12 and Table 6.

For unmodified POM_C and all composite samples, the course of the mechanical loss coefficient (tanδ) in the function of temperature shows three peaks corresponding to the three relaxations occurring in POM. For unmodified POM_C, the temperature values corresponding to relaxation effects are –60.6 °C (γ), –3.3 °C (β), and 115.7 °C (α), and are similar to the values reported in the literature [47]. Some differences in these temperatures may result, among others, from the oscillation frequency values that were

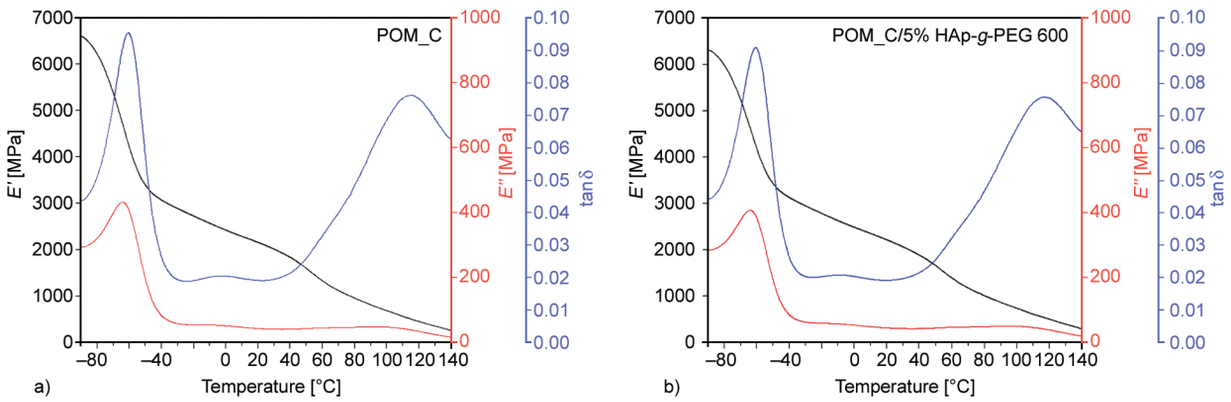

Figure 12. Dependence of the storage modulus E', loss modulus E'' and tan δ *vs.* temperature for POM_C (a) and POM_C composites with and 5.0% HAp-*g*-PEG 600 (b).

Table 6. Relaxation temperatures of POM_C and POM_C composites with 1.0 and 5.0% HAp-*g*-PEG 600, HAp-*g*-PEG 2000 and HAp-*g*-PEG 6000.

Sample	γ [°C]	β [°C]	α [°C]
POM_C	–60	–3	116
POM_C/1.0% HAp-*g*-PEG 600	–61	–5	117
POM_C/5.0% HAp-*g*-PEG 600	–61	–9	117
POM_C/1.0% HAp-*g*-PEG 2000	–60	–7	116
POM_C/5.0% HAp-*g*-PEG 2000	–60	–6	118
POM_C/1.0% HAp-*g*-PEG 6000	–61	–6	116
POM_C/5.0% HAp-*g*-PEG 6000	–61	–3	118

used during the DMA measurements [48]. The first relaxation, γ, is generally considered as the POM glass transition temperature, related to local movements of the POM segments forming amorphous areas [49].

Based on the obtained thermomechanical results, it has been found that the addition of HAp-*g*-PEG did not have a significant effect on the glass transition temperature (T_g for the γ transformation) of POM_C. A slightly greater effect was observed for the remaining POM_C relaxations, where the addition of the hybrid filler caused a slight decrease of the β relaxation temperature in the crystalline phase by a maximum of 5.4 °C and a slight increase in the α relaxation temperature – also in the amorphous phase, increasing its value by a maximum of 2.3 °C. The addition of HAp-*g*-PEG decreased the value of the mechanical loss coefficient (tanδ), which indicates a weaker ability to dampen vibrations in the tested composites compared to the unmodified POM_C. Moreover, the storage modulus (E'), representing the values of energy storage and return during successive deformation cycles, decreased with increasing temperature for all analyzed samples. This effect is associated with an increase in the mobility of the polymer chain segments with increasing temperature [50]. At –90 °C, for POM_C, the storage modulus reaches a maximum value of 6593 MPa. With increasing temperature, there is a sharp decrease in the E' value, down to 3392 MPa (at –50 °C), associated with the transition of the polymer from the glassy state, where the polymer is hard and brittle, to the elastic state. With an increase in temperature, a further, less rapid decrease of the storage modulus E' to 1730 MPa (at 45 °C) was recorded, followed by another decrease in E' due to the relaxation of the crystalline phase. This transformation (called $T_{\alpha c}$) takes place in some semicrystalline polymers and is associated with the appearance of limited movements of the polymer chain segments within the folded crystals. It is accompanied by a decrease in the value of the E', which occurs before the polymer melting process [51]. Samples containing the addition of HAp-*g*-PEG have a slightly lower storage modulus than pure POM_C, which indicates a slight decrease in the stiffness of the tested composites, but the shape of the E' curves remains similar to pure POM_C. The last parameter measured in DMA is the loss modulus (E''), which reaches its maximum at the glass transition temperature of the polymer [52]. For pure POM_C, the maximum value of E is 432 MPa (at –64.3 °C). The maximum temperature E'' is lower than the maximum temperature read from the maximum tanδ, which is also a characteristic phenomenon in DMA measurements for polymers. For composite materials, the maximum value of the loss modulus reflecting the amount of energy dissipated by the material during deformation was lower than for pure POM_C. The E'' value for POM_C/5.0% HAp-*g*-PEG 2000 decreased the most

by as much as 15%. As it can be seen for this sample, the highest relaxation/glass transition temperatures have been found that suggest the stiffest material with the lowest ability for vibration damping. In summary, POM_C and its composites were characterized by viscoelastic properties, as evidenced by the presence of the $E' \neq 0$ component and the $E'' \neq 0$ component. All of the tested materials were characterized by the presence of three relaxations occurring during material heating related to the relaxation of both the crystalline and amorphous phases. The addition of HAp-*g*-PEG did not significantly affect the T_g temperature value, which, according to the literature data for POM_C, ranges from -65 to -60 °C [53].

4. Conclusions

In the presented work, the influence of the chemical composition of the hybrid inorganic-organic HAp-based additive (HAp-*g*-PEG) on selected properties of POM composites was investigated. Among all the diisocyanates tested (HDI, MDI, HMDI, and iPDI), HDI turned out to be the most reactive. It was observed that the average molecular weight of PEG had a much smaller influence on the course of the grafting process, although the best results were obtained for the shortest chains (PEG 600) due to the highest concentration of their hydroxyl groups. On the basis of the obtained results, for further research, the HAp-HDI-PEG 600, HAp-HDI-PEG 2000, and HAp-HDI-PEG 6000 hybrid systems were selected, which were introduced into the polyoxymethylene matrix, both POM_C and POM_H, in an amount from 0.5 to 10.0 wt% based on the content of pure HAp. TEM confirmed the uniform distribution of HAp-*g*-PEG hybrid additives, even with a large amount of additive. DSC tests did not show any significant effect on the key processing parameters, *i.e.*, melting point and supercooling, which allows the processing parameters to be maintained for all samples.

FTIR-ATR analysis confirmed the complexity of the crystal forms formed in POM_C crystallization from the melt. This study did not show any changes in the POM crystallization method under the influence of the additives used.

The study of the crystallization kinetics showed a three-dimensional process of POM crystals' growth in the form of spherulites. The addition of HAp-*g*-PEG in POM_C significantly accelerated the crystallization process. The results of the microstructure analysis of POM_C and its composites using SEM and AFM methods confirmed the three-dimensional crystallization of POM_C chains in the form of spherulites. DMA method allowed for the determination of the POM_C glass transition temperature in the tested composites. Noteworthy, no significant influence of each of the additives used, regardless of its type and amount, on the glass transition temperature was observed.

Acknowledgements

The authors are grateful to the Polish National Science Centre for financial support under the Contract No. UMO-2016/21/B/ ST8/00449. This work was also supported from the subsidy of the Ministry of Education and Science for the AGH University of Science and Technology in Kraków (Project No 16.16.160.557).

References

[1] Masamoto J., Iwaisako T., Chohno M., Kawamura M., Ohtake J., Matsuzaki K.: Development of a new advanced process for manufacturing polyacetal resins. Part I. Development of a new process for manufacturing highly concentrated aqueous formaldehyde solution by methylal oxidation. Journal of Applied Polymer Science, **50**, 1299–1305 (1993). https://doi.org/10.1002/app.1993.070500801

[2] Lüftl S., Visakh P. M., Chandran S.: Polyoxymethylene handbook: Structure, properties, applications and their nanocomposites. Wiley, Hoboken (2014).

[3] Pielichowska K.: Polyacetal. in 'Handbook of thermoplastics' (eds.: Olabisi O., Adewale K.) CRC Press, Boca Raton (2015).

[4] Tashiro K.: Crystal structure and crystallization behavior of pom and its microscopically–viewed relation with the physical and thermal properties on the basis of X-ray scattering, vibrational spectroscopy and lattice dynamical theory. in 'Polyoxymethylene handbook: Structure, properties, applications and their nanocomposites' (eds.: Lüftl S., Visakh P. M., Chandran S.) Wiley, Hoboken, 193–226 (2014). https://doi.org/10.1002/9781118914458.ch7

[5] Raimo M.: Impact of thermal properties on crystalline structure, polymorphism and morphology of polymer matrices in composites. Materials, **14**, 2136 (2021). https://doi.org/10.3390/ma14092136

[6] Raimo M.: Structure and morphology of polyoxymethylene. in 'Polyoxymethylene handbook: Structure, properties, applications and their nanocomposites' (eds.: Lüftl S., Visakh P. M., Chandran S.) Wiley, Hoboken, 163–191 (2014). https://doi.org/10.1002/9781118914458.ch6

[7] Hama H., Tashiro K.: Structural changes in non-isothermal crystallization process of melt-cooled polyoxymethylene[II] evolution of lamellar stacking structure derived from SAXS and WAXS data analysis. Polymer, **44**, 2159–2168 (2003). https://doi.org/10.1016/S0032-3861(03)00093-4

[8] Hama H., Tashiro K.: Structural changes in non-isothermal crystallization process of melt-cooled polyoxymethylene. [I] Detection of infrared bands characteristic of folded and extended chain crystal morphologies and extraction of a lamellar stacking model. Polymer, **44**, 3107–3116 (2003). https://doi.org/10.1016/S0032-3861(03)00207-6

[9] Tashiro K.: Recognition of high sensitivity of vibrational spectroscopy in study of higher-order structure of polymers. J-Stage, **58**, 253–261 (2002). https://doi.org/10.2115/fiber.58.253

[10] Pielichowska K.: Polyoxymethylene processing. in 'Polyoxymethylene handbook: Structure, properties, applications and their nanocomposites' (eds.: Lüftl S., Visakh P. M., Chandran S.) Wiley, Hoboken, 107–151 (2014). https://doi.org/10.1002/9781118914458.ch4

[11] Zeng Y., Liu Y., Wang L., Huang H., Zhang X., Liu Y., Min M., Li Y.: Effect of silver nanoparticles on the microstructure, non-isothermal crystallization behavior and antibacterial activity of polyoxymethylene. Polymers **12**, 424 (2020). https://doi.org/10.3390/polym12020424

[12] Slouf M., Krejcikova S., Vackova T., Kratochvil J., Novak L.: *In situ* observation of nucleated polymer crystallization in polyoxymethylene sandwich composites. Frontiers in Materials, **2**, 23 (2015). https://doi.org/10.3389/fmats.2015.00023

[13] de Souza Santos C. L., Dias M. L., da Silva M. H. P.: Polyoxymethylene/graphene nanocomposites: Thermal, crystallization, melting and rheological behavior. Journal of Composite Materials, **55**, 1485–1498 (2020). https://doi.org/10.1177/0021998320972179

[14] Jiao Q., Chen Q., Wang L., Chen H., Li Y.: Investigation on the crystallization behaviors of polyoxymethylene with a small amount of ionic liquid. Nanomaterials, **9**, 206 (2019). https://doi.org/10.3390/nano9020206

[15] Navarro-Baena I., Arrieta M. P., Mujica-Garcia A., Sessini V., Lopez D., Kenny J. M., Peponi L.: Thermal degradation effects on polyurethanes and their nanocomposites. in 'Reactions and mechanisms in thermal analysis of advanced materials' (eds.: Tiwari A., Raj B.) Wiley, Hoboken, 165–189 (2015).

[16] Chattopadhyay D. K., Webster D. C.: Thermal stability and flame retardancy of polyurethanes. Progress in Polymer Science, **34**, 1068–1133 (2009). https://doi.org/10.1016/j.progpolymsci.2009.06.002

[17] Lee S. C., Choi H. W., Lee H. J., Kim K. J., Chang J. H., Kim S. Y., Choi J., Oh K-S., Jeong Y-K.: *In-situ* synthesis of reactive hydroxyapatite nano-crystals for a novel approach of surface grafting polymerization. Journal of Materials Chemistry, **17**, 174–180 (2007). https://doi.org/10.1039/B611401F

[18] Edwin N., Saranya S., Wilson P.: Strontium incorporated hydroxyapatite/hydrothermally reduced graphene oxide nanocomposite as a cytocompatible material. Ceramics International, **45**, 5475–5485 (2019). https://doi.org/10.1016/j.ceramint.2018.12.002

[19] Malakooti S., Rostami S., Churu H. G., Luo H., Clark J., Casarez F., Rettenmaier O., Daryadel S., Minary-Jolandan M., Sotiriou-Leventis C., Leventis N., Lu H.: Scalable, hydrophobic and highly-stretchable poly(isocyanurate–urethane) aerogels. RSC Advances, **8**, 21214–21223 (2018). https://doi.org/10.1039/C8RA03085E

[20] Mahou R., Wandrey C.: Versatile route to synthesize heterobifunctional poly(ethylene glycol) of variable functionality for subsequent PEGylation. Polymers, **4**, 561–589 (2012). https://doi.org/10.3390/polym4010561

[21] Dust J. M., Fang Z. H., Harris J. M.: Proton NMR characterization of poly(ethylene glycols) and derivatives. Macromolecules, **23**, 3742–3746 (1990). https://doi.org/10.1021/ma00218a0105

[22] Fu H., Gao H., Wu G., Wang Y., Fan Y., Ma J.: Preparation and tunable temperature sensitivity of biodegradable polyurethane nanoassemblies from diisocyanate and poly(ethylene glycol). Soft Matter, **7**, 3546–3552 (2011). https://doi.org/10.1039/C0SM01350A

[23] Kolmas J., Kolodziejski W.: Inverse $^{31}P \rightarrow {}^{1}H$ NMR cross-polarization in hydrated nanocrystalline calcium hydroxyapatite. Chemical Physics Letters, **554**, 128–132 (2012). https://doi.org/10.1016/j.cplett.2012.10.025

[24] Pielichowska K.: The influence of molecular weight on the properties of polyacetal/hydroxyapatite nanocomposites. Part 1. Microstructural analysis and phase transition studies. Journal of Polymer Research, **19**, 9775 (2012). https://doi.org/10.1007/s10965-011-9775-3

[25] Pielichowska K., Szczygielska A., Spasówka E.: Preparation and characterization of polyoxymethylene-copolymer/hydroxyapatite nanocomposites for long-term bone implants. Polymers for Advanced Technologies, **23**, 1141–1150 (2012). https://doi.org/10.1002/pat.2012

[26] Król-Morkisz K., Karaś E., Majka T. M., Pielichowski K., Pielichowska K.: Thermal stabilization of polyoxymethylene by PEG-functionalized hydroxyapatite: Examining the effects of reduced formaldehyde release and enhanced bioactivity. Advances in Polymer Technology, **2019**, 9728637 (2019). https://doi.org/10.1155/2019/9728637

[27] Król-Morkisz K., Pielichowska K.: Thermal decomposition of polymer nanocomposites with functionalized nanoparticles. in 'Polymer composites with functionalized nanoparticles' (eds.: Pielichowski K., Majka T. M.) Elsevier, Amsterdam 405–435 (2019). https://doi.org/10.1016/B978-0-12-814064-2.00013-5

[28] Pielichowski K., Flejtuch K.: Differential scanning calorimetry studies on poly(ethylene glycol) with different molecular weights for thermal energy storage materials. Polymers for Advanced Technologies, **13**, 690–696 (2002). https://doi.org/10.1002/pat.276

[29] Pielichowska K., Bieda J., Szatkowski P.: Polyurethane/graphite nano-platelet composites for thermal energy storage. Renewable Energy, **91**, 456-465 (2016). https://doi.org/10.1016/j.renene.2016.01.076

[30] Król-Morkisz K., Karaś E., Majka T. M., Pielichowski K.; Pielichowska K.: Thermal stabilization of polyoxymethylene by PEG-functionalized hydroxyapatite: Examining the effects of reduced formaldehyde release and enhanced bioactivity. Advances in Polymer Technology, **2019**, 9728637 (2019). https://doi.org/10.1155/2019/9728637

[31] Rahman M. S., Shaislamov U., Yang J-K., Kim J-K., Yu Y. H., Choi S., Lee H-J.: Effects of electron beam irradiation on tribological and physico-chemical properties of polyoxymethylene copolymer (POM-C). Nuclear Instruments and Methods in Physics Research Section B: Beam Interactions with Materials and Atoms, **387**, 54–62 (2016). https://doi.org/10.1016/j.nimb.2016.10.001

[32] Li Y., Zhou T., Chen Z., Hui J., Li L., Zhang A.: Non-isothermal crystallization process of polyoxymethylene studied by two-dimensional correlation infrared spectroscopy. Polymer, **52**, 2059–2069 (2011). https://doi.org/10.1016/j.polymer.2011.03.007

[33] Kurosu H., Komoto T., Ando I.: ^{13}C NMR chemical shift and crystal structure of polyoxymethylene in the solid state. Journal of Molecular Structure, **176**, 279–283 (1988). https://doi.org/10.1016/0022-2860(88)80247-3

[34] Matsumoto A., Egawa Y., Matsumoto T., Horii F.: Miscibility of polyoxymethylene blends as revealed by high-resolution solid-state ^{13}C-NMR spectroscopy. Polymers for Advanced Technologies, **8**, 250–256 (1997). https://doi.org/10.1002/(SICI)1099-1581(199704)8:4<250::AID-PAT636>3.0.CO;2-9

[35] Gupta S., Yuan X., Chung T. C. M., Cakmak M., Weiss R. A.: Isothermal and non-isothermal crystallization kinetics of hydroxyl-functionalized polypropylene. Polymer, **55**, 924–935 (2014). https://doi.org/10.1016/j.polymer.2013.12.063

[36] Avrami M.: Kinetics of phase change. I General theory. The Journal of Chemical Physics, **7**, 1103–1112 (1939). https://doi.org/10.1063/1.1750380

[37] Xu W-B., He P-S.: Crystallization characteristics of polyoxymethylene with attapulgite as nucleating agent. Polymer Engineering and Science, **41**, 1903–1912 (2001). https://doi.org/10.1002/pen.10887

[38] Mandelkern L.: Crystallization of polymers: Kinetics and mechanisms. Cambridge University Press, Cambridge (2004).

[39] Gedde U. W., Hedenqvist M. S.: Fundamental polymer science. Springer, Cham (2019).

[40] Xu W., He P.: Isothermal crystallization behavior of polyoxymethylene with and without nucleating agents. Journal of Applied Polymer Science, **80**, 304–310 (2001). https://doi.org/10.1002/1097-4628(20010411)80:2<304::AID-APP1100>3.0.CO;2-N

[41] Wu T-M., Chen E-C.: Crystallization behavior of poly (ε-caprolactone)/multiwalled carbon nanotube composites. Journal of Polymer Science Part B: Polymer Physics, **44**, 598–606 (2006). https://doi.org/10.1002/polb.20722

[42] Pracella M., Chionna D., Anguillesi I., Kulinski Z., Piorkowska E.: Functionalization, compatibilization and properties of polypropylene composites with hemp fibres. Composites Science and Technology, **66**, 2218–2230 (2006). https://doi.org/10.1016/j.compscitech.2005.12.006

[43] Plans J., MacKnight W. J., Karasz F. E.: Equilibrium melting point depression for blends of isotactic polystyrene with poly(2,6-dimethylphenylene oxide). Macromolecules, **17**, 810–814 (1984). https://doi.org/10.1021/ma00134a048

[44] Lee J. H., Park S. H., Kim S. H., Ito H.: Replication and surface properties of micro injection molded PLA/MWCNT nanocomposites. Polymer Testing, **83**, 106321 (2020). https://doi.org/10.1016/j.polymertesting.2019.106321

[45] Hoffman J. D.: Regime III crystallization in melt-crystallized polymers: The variable cluster model of chain folding. Polymer, **24**, 3–26 (1983). https://doi.org/10.1016/0032-3861(83)90074-5

[46] Li J., Fang Z., Zhu Y., Tong L., Gu A., Liu F.: Isothermal crystallization kinetics and melting behavior of multiwalled carbon nanotubes/polyamide-6 composites. Journal of Applied Polymer Science, **105**, 3531–3542 (2007). https://doi.org/10.1002/app.24606

[47] Psarras G. C., Siengchin S., Karahaliou P. K., Georga S. N., Krontiras C. A., Karger-Kocsis J.: Dielectric relaxation phenomena and dynamics in polyoxymethylene/polyurethane/alumina hybrid nanocomposites. Polymer International, **60**, 1715–1721 (2011). https://doi.org/10.1002/pi.3136

[48] Keating M. Y., Sauer B. B., Flexman E. A.: Dynamic mechanical characterization of relaxations in poly(oxymethylene), miscible blends, and oriented filaments. Journal of Macromolecular Science Part B, **36**, 717–732 (1997). https://doi.org/10.1080/00222349708212398

[49] Karahaliou P. K., Kerasidou A. P., Georga S. N., Psarras G. C., Krontiras C. A., Karger-Kocsis J.: Dielectric relaxations in polyoxymethylene and in related nanocomposites: Identification and molecular dynamics. Polymer, **55**, 6819–6826 (2014). https://doi.org/10.1016/j.polymer.2014.10.056

[50] Yang W., Wang X-L., Yan X., Guo Z.: Toughened polyoxymethylene by polyolefin elastomer and glycidyl methacrylate grafted high-density polyethylene. Polymer Engineering & Science, **57**, 1119–1126 (2017). https://doi.org/10.1002/pen.24489

[51] van Krevelen D. W., te Nijenhuis K.: Properties of polymers: Their correlation with chemical structure; Their numerical estimation and prediction from additive group contributions. Elsevier, Amsterdam (2009).

[52] Matsuoka S.: Thermodynamic theory of viscoelasticity. Journal of Thermal Analysis, **46**, 985–1010 (1996). https://doi.org/10.1007/BF01983616

[53] Archodoulaki V-M., Lüftl S.: Thermal properties and flammability of polyoxymethylene. in 'Polyoxymethylene handbook: Structure, properties, applications and their nanocomposites' (eds.: Lüftl S., Visakh P. M., Chandran S.) Wiley, Hoboken, 257–275 (2014). https://doi.org/10.1002/9781118914458.ch10